

Characterizing the Quaternary expression of active faulting along the Olinghouse, Carson, and Wabuska lineaments of the Walker Lane

Xinnan Li^{1,2}, Weiliang Huang^{2,3,*}, Ian K.D. Pierce^{2,4,*}, Stephen J. Angster^{2,4,*}, and Steven G. Wesnousky^{2,4,*}

¹State Key Laboratory of Earthquake Dynamics, Institute of Geology, China Earthquake Administration, No. 1, Huayanli, Chaoyang District, Beijing 100029, China

²Center for Neotectonics Studies, University of Nevada, Reno, MS 169, 1664 N Virginia Street, Reno, Nevada 89557, USA

³College of Geologic Engineering and Surveying of Chang'an University, 126 Yanta Avenue, Yanta District, Xi'an, Shaanxi Province, China

⁴Nevada Seismological Laboratory, University of Nevada, Reno, MS 169, 1664 N. Virginia Street, Reno, Nevada 89557, USA

ABSTRACT

The northern Walker Lane (southwestern USA) accommodates ~5–7 mm/yr of right-lateral Pacific–North America relative plate motion. The north-west trend of major right-lateral faults in the Walker Lane is interrupted by the presence of northeast-striking left-lateral faults within the Carson and Excelsior domains. Previous studies in the Carson domain have suggested that left-lateral slip on the northeast-striking Olinghouse, Carson, and Wabuska lineaments accommodates Walker Lane transtensional dextral shear through the clockwise rotation of intervening crustal blocks. Our observations confirm and document the presence of late Pleistocene–Holocene faulting along each of these lineaments. Fault scarps along the Carson and Wabuska lineaments are discontinuous and sparse, and show evidence for left-lateral faulting, locally including linear fault traces, alternating scarp face directions, and lateral offsets of small gullies and ridges. The trends of scarps that define these lineaments link at their western ends with north-trending active normal faults. In this manner, it appears that the 5–7 mm/yr of right slip taking place across the northern Walker Lane is being accommodated by the combined processes of basin opening in the west and block rotation to the east. This mode of slip transfer differs from the Excelsior domain, where active left-slip faults and clockwise rotation of crustal blocks are confined to, and the result of, a distinct right step between right-lateral faults of the southern Walker Lane and central Walker Lane, respectively. The observation of these apparently diverse modes of development of left-slip faults and vertical axis rotations provides an example of the complexity that may be expected in the structural development of continental shear zones that have been characterized by transtension.

*E-mail: haungweiliang1987@gmail.com, ian@nevada.unr.edu, sangster@nevada.unr.edu, wesnousky@unr.edu

INTRODUCTION

The Walker Lane (southwestern USA) is a major intraplate shear zone defined by a northwest-trending zone of discontinuous active faults, basins, and ranges that is between the Sierra Nevada to the west and the north-northeast-striking faults and ranges of the Basin and Range to the east (Fig. 1). It is unique in its width and discontinuous character when compared to other major continental strike-slip faults observed around the globe, including well-known examples such as the San Andreas, which is located just to the west (Fig. 1), the Anatolian fault of Turkey (e.g., Şengör et al., 2005), the Altyn Tagh of Tibet (e.g., Yin et al., 2002), the Denali fault system of Alaska (e.g., Hickman et al., 1978), and the Alpine fault system of New Zealand (Zealandia) (e.g., Norris and Toy, 2014; Mortimer et al., 2017). Cumulative right-lateral slip taken up by the Walker Lane ranges from ~30 km in the north to >50 km in the south. Geodesy shows the Walker Lane corresponds to a well-defined zone of northwest-directed transtensional dextral shear ranging from ~12 mm/yr in the south to ~5–7 mm/yr in the north (Bennett et al., 2003; Hammond and Thatcher, 2007). In Wesnousky (2005b) it was conjectured that the discontinuous nature of faulting in the Walker Lane as compared to the San Andreas may be attributed to the greater cumulative offset having accrued along the San Andreas, and that the San Andreas is transpressional along most of its length, in contrast to the transtension that characterizes the Walker Lane. In this regard, efforts to characterize the varying modes of deformation observed in the Walker Lane may provide clues to understanding the early development of continental shear zones exhibiting larger displacement during periods of time in their development where observations show they were characterized by transtension. The Carson and Excelsior domains of the Walker Lane are each characterized by the presence of left-lateral faults that strike approximately transverse to the general northwest trend of the Walker Lane. In this paper we focus on presenting new observations bearing on the recency, sense, and style of slip of faults within the Carson domain. These observations are then compared to those of others collected within the Excelsior domain to show that the developments of the left-lateral systems differ significantly in the two regions.

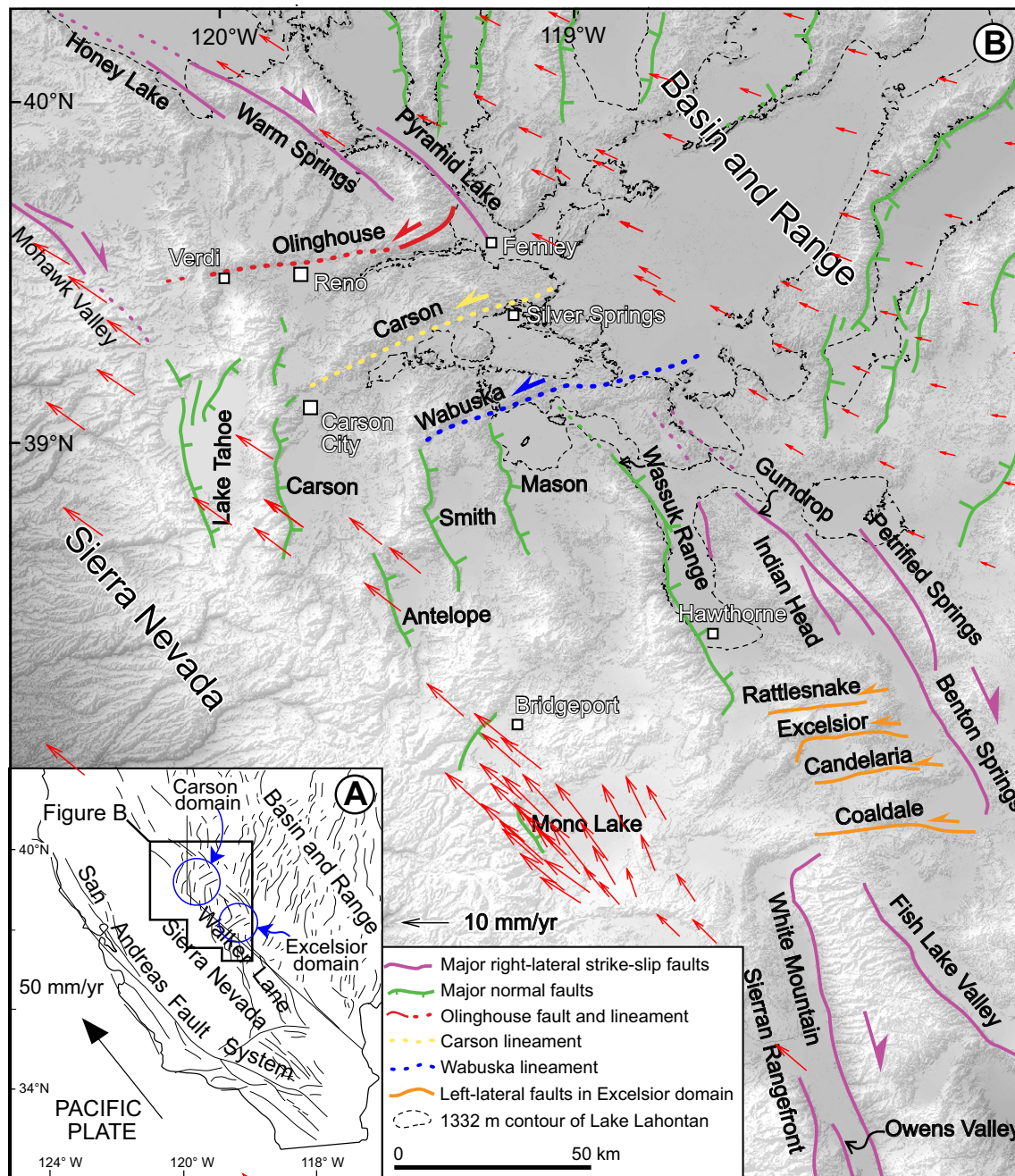


Figure 1. Tectonic setting of the study area. (A) Regional fault map showing faults of the San Andreas, Walker Lane, and Basin and Range. Locations of the Carson and Excelsior domains are outlined by blue circles. (B) Enlarged view of the Walker Lane displaying physiographic and fault trends. The northeast-trending Olinghouse (red), Carson (yellow), and Wabuska (blue) lineaments are the focus of this study. Normal faults (teeth on downthrown side) are green, right-lateral strike slip faults are magenta, and left-lateral strike-slip faults of Excelsior domain are orange. Thin dashed line is higheststand contour (1332 m) of pluvial Lake Lahontan. Red arrows are global positioning system velocity vectors plotted with respect to stable North America adapted from Hammond and Thatcher (2007).

The early recognition of the northwest-trending right-lateral strike-slip faulting (Callaghan and Gianella, 1935; Locke et al., 1940; Ferguson and Muller, 1949) and Stewart's (1980, 1985) and subsequent observations bearing on the complexity of deformation, have since been followed by numerous efforts to understand how shear strain is accommodated within the Walker Lane (e.g., Slemmons et al., 1979; Stewart, 1980, 1988; Dokka and Travis, 1990; Wesnousky and Jones, 1994; Dixon et al., 1995; Reheis and Dixon, 1996; Cashman and Fontaine, 2000; Oldow et al., 2001; Stockli et al., 2002; Surpless et al., 2002; Faulds et al., 2003; Unruh et al., 2003; Wesnousky, 2005a, 2005b; Henry et al., 2007; Faulds and Henry, 2008; Hoeft and Frankel, 2010; Wesnousky et al., 2012; Bormann et al., 2016). Stewart (1980, 1988) drew upon his observations and those of others to divide the Walker Lane into distinct structural domains and blocks. Two of the regions contain northeast-trending sinistral structures within the Walker Lane, that Stewart (1988) labeled the Excelsior and Carson domains (Fig. 1). The more southern Excelsior domain includes the Rattlesnake, Excelsior, and Candelaria faults, the neotectonic characteristics of which were described in some detail in Wesnousky (2005a, 2005b). To the north, the Carson domain encompasses the east-northeast-striking Olinghouse, Carson, and Wabuska faults and lineaments, along with a series of five subparallel north-striking fault-bounded basins: Lake Tahoe, Carson, Smith, Antelope, and Mason Valleys. In each of the regions, investigators have concluded that the left-slip faults are coupled with clockwise vertical axis rotation of the crust that serves to accommodate the northwest-directed right-lateral shear of the Walker Lane (e.g., Cashman and Fontaine, 2000; Wesnousky, 2005a; Carlson et al., 2013; Carlson and Faulds, 2016; Nagorsen-Rinke et al., 2013).

Here we combine new observations with the old to describe the neotectonic characteristics of the Olinghouse, Carson, and Wabuska lineaments. These observations provide the basis to compare and contrast the characteristics of the active faulting within the Carson domain to the Excelsior domain, and discuss the role they play in accommodating the dextral shear within the Walker Lane. We first discuss the resources and methods we employ, and follow with a review and reexamination of the physiographic and neotectonic characteristics of the Olinghouse, Carson, and Wabuska faults and lineaments.

■ RESOURCES AND METHODS

Our descriptions of faulting characteristics along each of the faults and lineaments are derived from the analysis of large-scale (1:12,000), low-sun-angle black and white air photos and lidar (light detection and ranging) data (0.5 m/pixel) acquired with funding for this project through the National Center for Airborne Laser Mapping, and structure-from-motion (SfM) models developed for specific sites. Our primary goal was to look for evidence for the timing and kinematics of Quaternary faulting along each of these lineaments. Where instructive, observations are synthesized onto maps, which show the distribution of Quaternary deposits and style of faulting.

To provide regional reference to the interaction of the faults with Quaternary deposits, we constructed small-scale generalized surficial maps along the

Wabuska and Carson lineaments. The surficial Quaternary maps are developed from our analysis of available black and white air photo imagery of the region in conjunction with lidar data we collected for the project. Development of regional Quaternary maps generally follows that in Wesnousky (2005a). At the regional scale, mapped Quaternary deposits are broadly divided between lacustrine, eolian, flood plain, basin fill, and three mapped alluvial fan units; the subdivisions of the latter are based principally on variations in surficial characteristics, including the degree of dissection, elevation above modern stream grade, and tonal and textural differences observed in the field and on air photos and lidar images. The basis of this approach was described by Bull (1991), and has been used in various studies in this region (e.g., Bell et al., 2004; Wesnousky, 2005a; Koehler and Wesnousky, 2011; Sarmiento et al., 2011; Wesnousky and Caffee, 2011), and has more recently been adapted for lidar-based mapping of alluvial fan deposits (e.g., Frankel et al., 2007a, 2007b). For specific sites of study, the alluvial fan units are further subdivided to describe in better detail the character of faulting.

The oldest Quaternary deposits (Qo) are considered to be mid-Pleistocene and older in age. They are characterized by deeply dissected fan remnants commonly showing rounded or sharp crests that are ~10 m or more above modern stream grade, and are separated from younger depositional surfaces. Depositional surfaces interpreted to be of intermediate age (Qi) generally are no more than ~10 m above modern stream grade, exhibit lesser amounts of dissection, and are more often characterized by relatively broader, smooth, and flat interfluvial fan remnants than younger surfaces. These intermediate-aged surfaces are modified by lacustrine shoreline processes when at or below the level of the ~1332 m Lahontan (ca. 15.5 ka) highstand (Adams and Wesnousky, 1999), and so are generally considered here to be mid- to latest Pleistocene in age. The youngest fan deposits (Qy) include the undissected active fan and wash surfaces, which exhibit levee and channel or fresh bar and swale topography and few, if any, well-defined post-abandonment drainage channels. These young fans frequently overtop or cut the Lahontan shoreline deposits and are thus considered to be latest Pleistocene–Holocene deposits. The absolute ages of these units are not known and are difficult to correlate between drainages due to differences in localized fan system development. These unit delineations and regional maps serve to provide a broad context to view the interaction of faults with alluvium and bedrock. For specific sites of study, the alluvial fan units are further subdivided to describe in better detail the character of faulting, and these subdivisions are described further herein.

To further illustrate the finer details at sites with subtle morphology, we developed high-resolution SfM surface models following methods similar to those in Angster et al. (2016), using aerial photographs obtained from an unmanned aerial vehicle (UAV) platform (DJI Phantom 3 Vision+, www.dji.com/phantom-2-vision-plus). Our models are georeferenced using the internal global positioning system (GPS) of the UAV, and then further rectified with measured ground control points using a Trimble R10 GPS (www.trimble.com) receiver. Agisoft Photoscan Pro software (www.agisoft.com) was used to process the air photos into dense point clouds, from which digital elevation

models (DEMs) were produced and then exported into ArcMap (desktop.arcgis.com/en/arcmap/) where hillshade, slope, and contour plots were produced. Topographic profiles across fault scarps were constructed using ArcMap, and vertical offsets were measured by fitting linear regressions to the surfaces on either side of the fault and measuring the vertical separation of the projections of the surfaces at the middle of the scarp (e.g., Hanks et al., 1984). The most recent version of LaDiCaoz_v2.1 was used to measure lateral displacements (Zielke et al., 2015; Haddon et al., 2016).

■ PUBLISHED AND NEW OBSERVATIONS

The physiographic map of Figure 1 displays the faults and lineaments that define the Carson and Excelsior domains of the Walker Lane. Prior work and observations collected along these faults and lineaments are described separately.

Olinghouse Fault and Lineament

Published Observations

Bonham's (1969) mapping shows a number of northeast-striking faults in bedrock between Reno and Fernley, Nevada, and is perhaps the first published acknowledgment of the presence of structures cutting transverse to the

northwest-trending strike-slip faults, which now define the Walker Lane. The Olinghouse lineament is physiographically expressed from west to east by the alignment of small hills west of the Verdi Range; the large south-facing escarpment of Peavine Peak; the left-lateral Olinghouse fault zone; and its intersection with the Pyramid Lake fault zone (Fig. 2). The lineament is associated with and named for the Quaternary active Olinghouse fault originally reported by Sanders and Slemmons (1979), and later mapped in detail and trenched by Briggs and Wesnousky (2001), who recorded late Pleistocene displacements. The fault trace displaces shoreline deposits of the ca. 15.5 ka high-stand of the pluvial Lake Lahontan (Adams and Wesnousky, 1999). Left-laterally offset debris flow levees and channel thalwegs and a small pushup within a right step along the fault zone are preserved along the fault zone (Briggs and Wesnousky, 2001). The trenches of Briggs and Wesnousky (2005), closest to the western end of the mapped trace, recorded 2 earthquakes; the first sometime after $19,800 \pm 630$ calibrated (cal) yr B.P. and the other after 1935 ± 70 cal yr B.P. This is in contrast to the 4 events that have occurred on the conjugate Pyramid Lake fault zone since ca. 15.5 ka (Briggs and Wesnousky, 2004). No Quaternary displacements have been observed farther west along the Olinghouse lineament. In summary: (1) Quaternary activity of the Olinghouse lineament is absent but for along the Olinghouse fault, (2) fewer earthquakes have occurred on the Olinghouse fault than on the Pyramid Lake fault in the past ~16 k.y., and (3) preservation of offset geomorphic features shows the fault to have produced left-lateral slip in the latest Pleistocene.

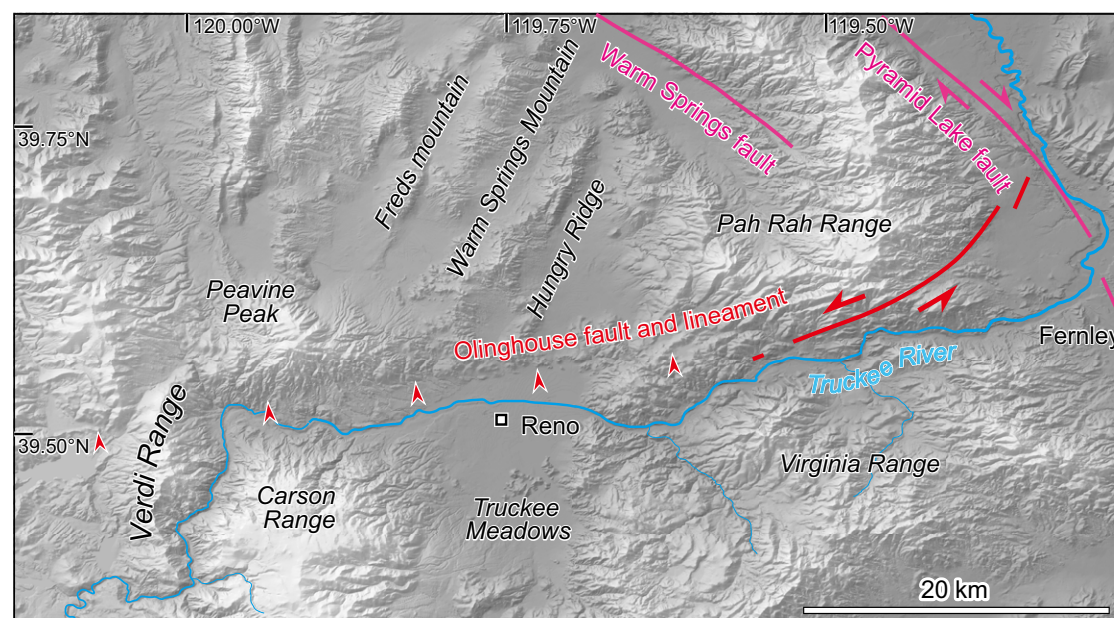


Figure 2. Close up of study area. The Olinghouse lineament is marked by small red arrows, and the left-lateral Olinghouse fault is marked by the solid red line. The Pyramid Lake and Warm Springs faults of the Northern California shear zone are shown as magenta lines.

Carson Lineament

Published Observations

The interpretation of the Carson lineament as a structural zone that has accommodated left-lateral displacement first appeared in Shawe (1965, figure 8 therein). The first recognition of faults along the lineament that displace young alluvium is generally attributed to Rogers (1975). The existence and presumed importance to active tectonics of the Carson lineament was implied in Slemmons et al. (1979, figure 1 therein) and Sanders and Slemmons (1979, figure 1 therein). Thereafter, the faults within the lineament that break Quaternary deposits first appeared and were briefly discussed in the reports attendant to the 1:250,000-scale maps of Bell (1981, 1984). This discontinuous trend of fault traces interpreted to break Quaternary deposits was likewise recorded and mapped at a similar scale in the geologic map of the Carson City quadrangle (Stewart, 1999). Detailed mapping of neotectonic features and displaced Quaternary deposits along the Carson lineament is absent from the literature. Larger scale imagery and maps are used here to provide a more detailed picture of the neotectonic and Quaternary characteristics of the lineament.

New Observations

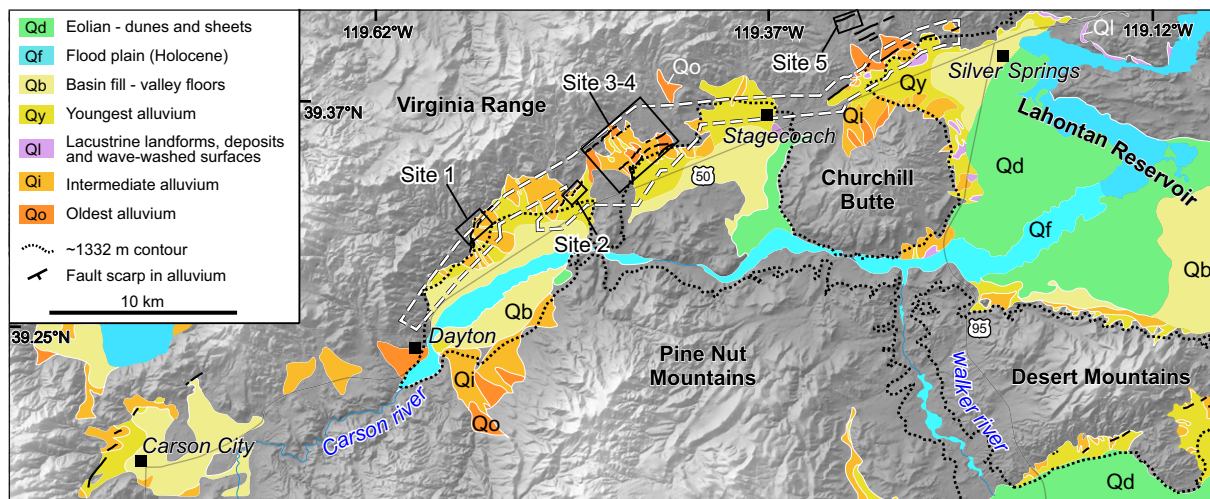
The traces of Quaternary fault scarps are shown upon a hillshade image and a simplified Quaternary map in Figure 3. The youngest alluvial units are generally fan and wash deposits, which have been deposited following the recession of the lake. These deposits frequently cut and override the shoreline deposits from the lake. Between Dayton and Silver Springs and along the

irregular southeastern flank of the Virginia Range, discontinuous fault scarps in Quaternary alluvium display a right-stepping en echelon pattern. No scarps are observed within the post-Lahontan surfaces, suggesting that displacement has not occurred since at least that time (15.5 ka). Fault scarps in the southwest corner of Figure 3, near Carson City and at the northern end of Carson Valley, have the same trend and intersect the more north-striking faults of Carson Valley to the south (Fig. 1). Multiple late Holocene displacements have been documented in trenches excavated across the range-bounding fault of Carson Valley, the Genoa fault (Ramelli et al., 1999), and equally young displacements have been interpreted for the scarps adjacent to Carson City (Trexler and Bell 1979; DePolo, 2014). Examination of the lidar data sets along the linear northern flank of the Desert Mountains and along the stretches of the Carson River adjacent to Churchill Butte and the Pine Nut Mountains (Fig. 3) failed to document any fault scarps cutting Quaternary deposits.

At Six Mile Canyon, northeast of Dayton, Nevada, evidence for repeated Quaternary displacements is preserved as progressively greater vertical offsets in older fan surfaces at site 1 (Figs. 3 and 4). On the north side of the drainage, an ~1–2 m scarp (fault strand f1 in Fig. 4B) is measured within a Qi pre-Lahontan alluvial surface (p3 in Figs. 4B, 4C). South of the drainage, a fluvial terrace (T2) is inset into a broad smooth Qo Pleistocene alluvial surface and truncated by an ~7.2 m scarp (fault strand f2; p2 in Figs. 4B, 4C), likely recording multiple displacements of similar size. The fault traces here lack evidence for lateral displacements, possibly due to the absence of appropriate markers that record left-lateral offset.

East of site 1, and shown in Figure 5, is a well-preserved fault scarp (site 2) that strikes southwest off a bedrock salient. This 1.4 m scarp is quite linear, and vertically displaces broad, smooth, and lightly dissected alluvial surfaces.

Figure 3. Map of Quaternary deposits along the Carson lineament shows site locations 1 through 5. Dashed white line outlines the extent of lidar (light detection and ranging) coverage. Black lines are active faults. Highstand contour (1332 m) of pluvial Lake Lahontan is thin dotted black line. Generalized map units: Qd—eolian dunes and sheets (green); Qf—Holocene flood-plain deposits (cyan); Qb—basin fill sediments (light yellow); Qy—latest Pleistocene–Holocene sediment (yellow); Qi—lacustrine deposits and wave-washed surfaces of Lake Lahontan; Oi—intermediate-aged (approximately mid- to late Pleistocene) alluvial surfaces (orange); and Qo—older Quaternary surfaces.



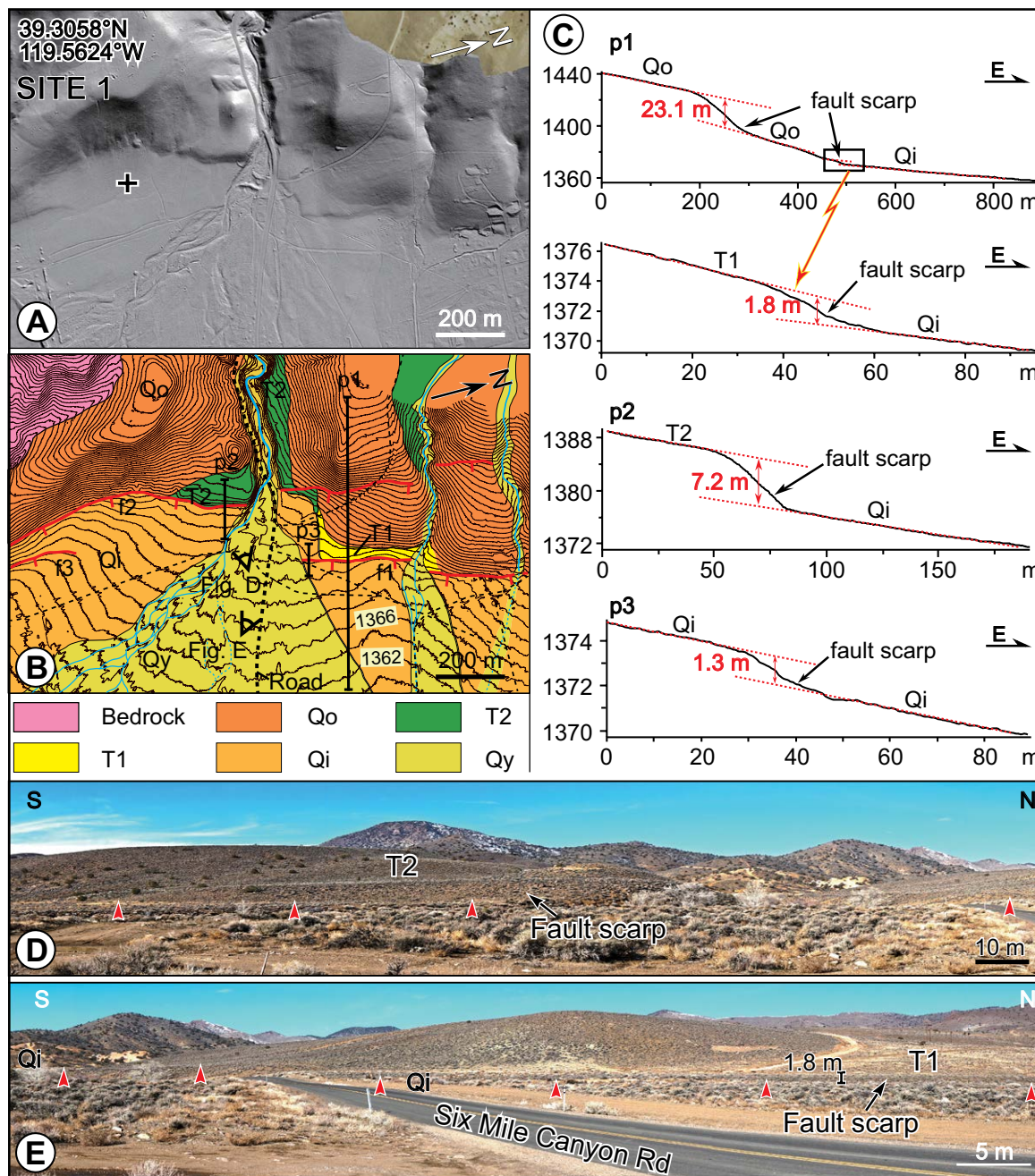


Figure 4. Displaced geomorphic features along the fault trace at site 1 (location outlined by box in Fig. 3). (A) Lidar (light detection and ranging) hillshade image. Geographic coordinate of plus sign is labeled. (B) Quaternary map of site 1 showing active fault scarps (red; tick marks on downthrown side). In addition to Quaternary units described in caption of Figure 3, units T1 and T2 are local fluvial terraces of younger and older relative age, respectively, and intermediate in age between Qo and Qi. Contour interval is 2 m. (C) Plots of topographic profiles along lines p1, p2, and p3 in B. Scarp heights are greater across increasingly older T1, T2, and surfaces. (D, E) Perspectives of photographs located in B. Red arrow points in each photo are located at bases of scarps. Bases of labels T1 and T2 are located on top of respective surfaces.

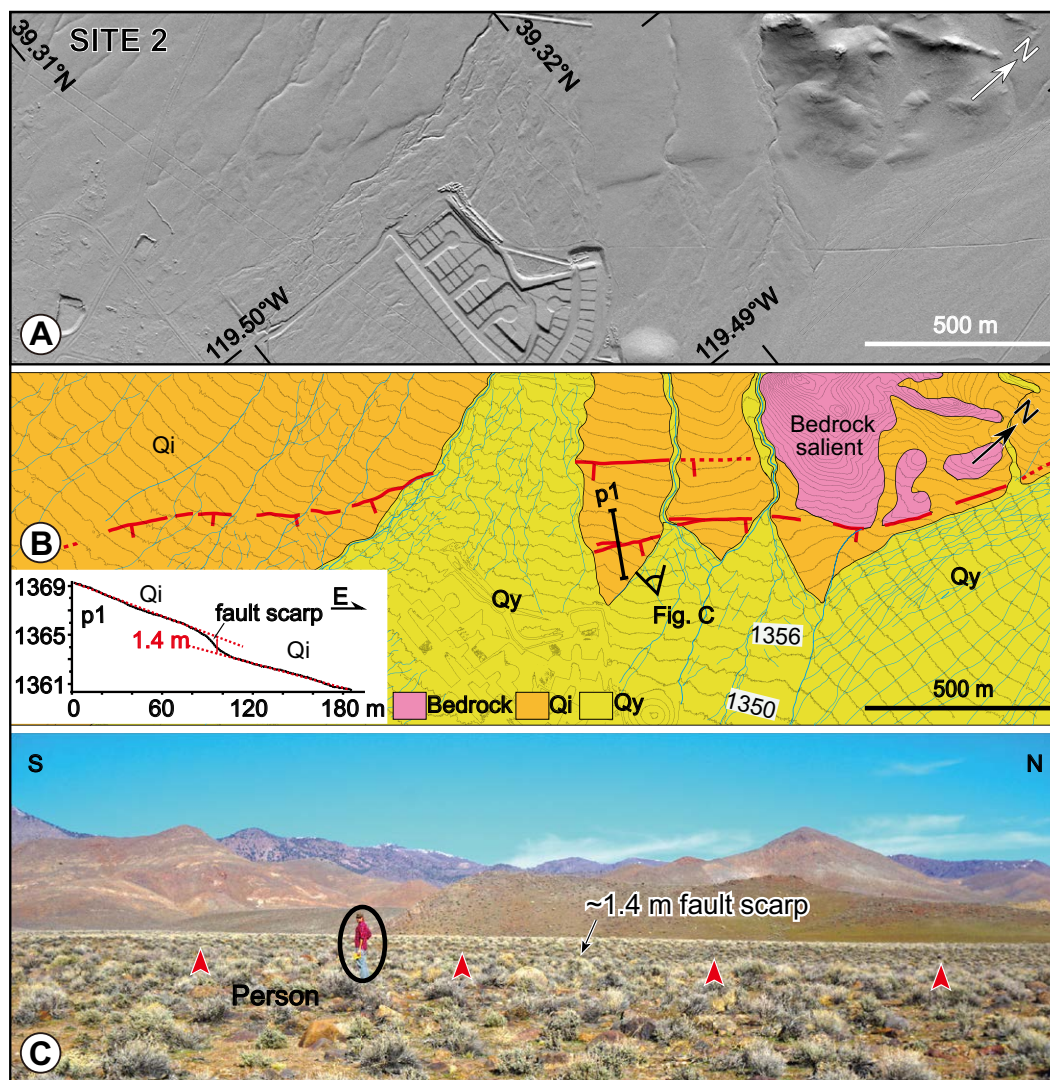


Figure 5. Geographic features along the fault trace at site 2 (location outlined by box in Fig. 3). (A) Lidar (light detection and ranging) hillshade image. (B) Quaternary map showing active fault scarps (red, tick marks on the downthrown side). Topographic profile along p1 in inset shows scarp height of 1.4 m. Contour interval is 2 m. Unit abbreviations as in Figure 3. (C) Photograph illustrates character of scarp in field. Points of red arrowheads located along base of the scarp (perspective of photo is shown in B).

This fault scarp is not present in adjacent younger surfaces (Qy), which have clear bar and swale topography. Based on the low slope angle of the scarp within the Qi deposits and the lack of scarp in more recent Qy fan deposits, the offset at site 2 (Fig. 5) predates the Holocene. Our observations along this structure are therefore consistent with relatively long recurrence intervals of ~10 k.y.

Northeast of the fault scarps in Figure 5 are sets of ~4 subparallel scarps that cut a several-kilometer-wide bajada (Figs. 3 and 6A). Each is labeled as trace 1, trace 2, and so on in Figures 6A, 6B, and 6E. The timing of displacements on these fault strands is in-part inferred by the remnants of the pluvial Lake Lahontan shorelines observed in the southeast portion of the maps. Lacustrine shoreline deposits with rounded clast-supported gravel are well preserved

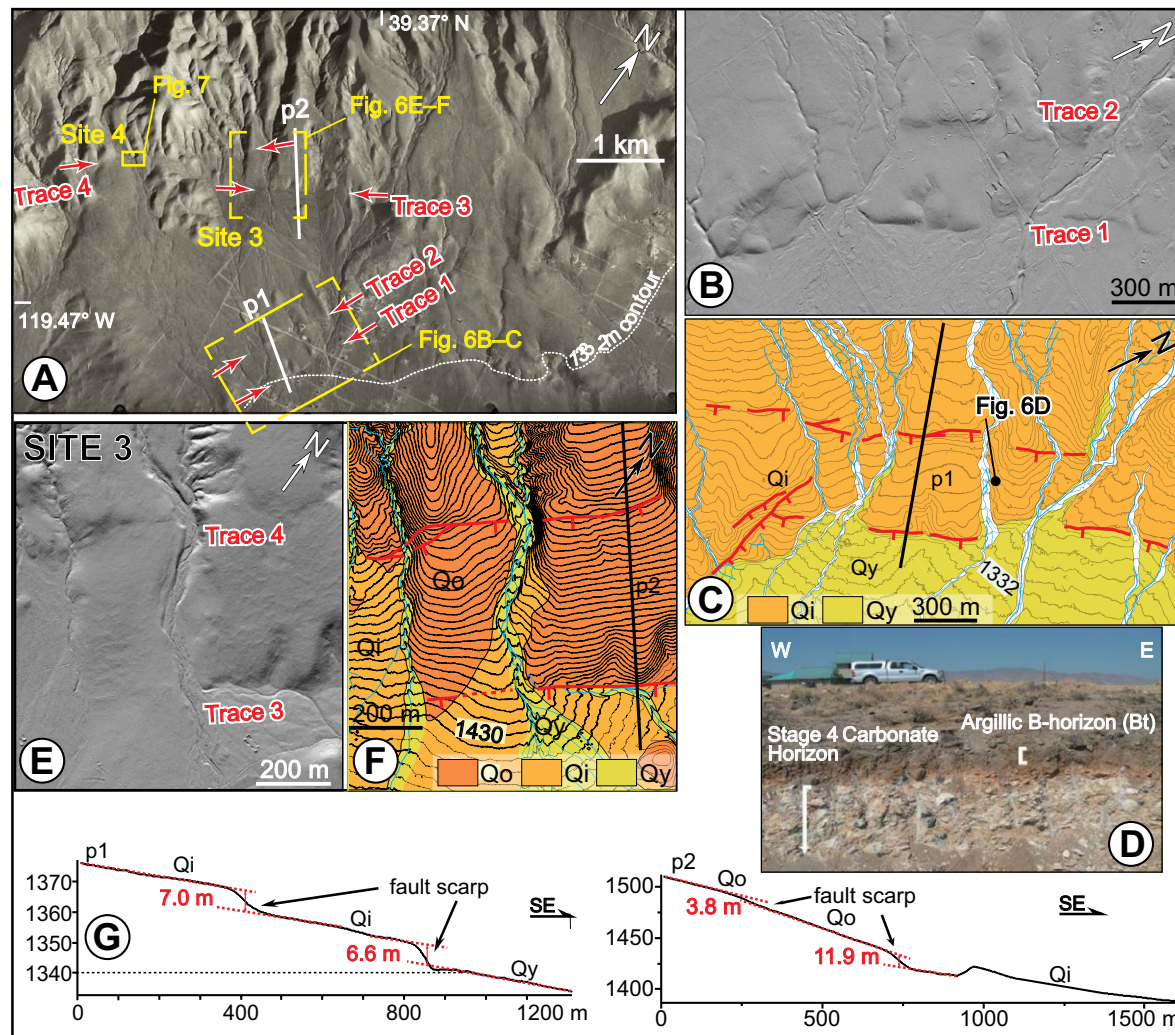


Figure 6. Displaced geomorphic features along southern Virginia Range-front. Unit abbreviations as in Figure 3. (A) Portion of 1:24,000-scale air photo. (Approximate area of image outlined by area labeled as sites 3 and 4 in Fig. 3). Fault scarps strike between pairs of oppositely facing red arrows and labeled as traces 1 to trace 4. (B, C) Hillshade image and Quaternary map of region outlined by yellow box at bottom of image shown in A. Fault scarps (red lines in C) are with ticks on downthrown side. Fault trace 1 may be modified by lacustrine processes at time of Lake Lahontan highstand. (D) Photo of argillic B-horizon and stage 4 carbonate horizon in an intermediate Qi fan surface. Location (39.349481°N, 119.453740°W) of photo is shown in A. (E, F) Hillshade image and Quaternary map of site 3. Mapping conventions as in B and C. Contour interval is 2 m. (G) Topography along profiles p1 and p2 illustrate scarp heights in each of the mapped areas.

along the 1332 m highstand contour, and a well-developed wave-modified scarp is located along much of this contour. Alluvial surfaces, which were cut or modified by the Lake Lahontan shoreline deposits, are thus interpreted to be older than ca. 15.5 ka.

Fault trace 1 (Figs. 6B, 6C) is west of the shoreline deposits described in the preceding paragraph. The southwestern end of the fault cuts an intermediate (Qi) fan surface with an ~6.6 m scarp (p1 in Figs. 6C, 6G), and parallels the 1332 m highstand (Figs. 6A, 6B). A road cut into the intermediate (Qi) fan

surface (Fig. 6D) revealed a strongly developed argillic B-horizon underlain by stage 4 carbonate horizon approaching 1 m in thickness. This amount of soil development requires that the fan surface has been stable since the mid-Pleistocene (e.g., Frankel et al., 2007a, 2007b; Koehler and Wesnousky, 2011). The trace 1 scarp bounding this surface on the southeast was likely modified by the shoreline processes. Shoreline deposits are not observed on the hanging wall of this section of the scarp, so it is possible that this fan and fault scarp are older than the highstand. The well-developed soil and the relatively small

offsets suggest a long recurrence interval of faulting and low vertical slip rate for this strand of the fault.

Fault trace 2 (Figs. 6B, 6C) strikes subparallel to trace 1 and is defined by ~7 m scarps (p1 in Figs. 6C, 6G) in intermediate (Qi) fan and pediment surfaces that are above the 1332 m contour (Figs. 6A, 6B). At the southwestern end of fault trace 2, and a few hundred meters south of the soil exposure shown in Figure 6D, the fault is expressed within the same wave-modified surface described to be cut by fault trace 1. This observation along with the subdued nature of the scarp, as illustrated by p1 in Figure 6G, suggests that the most recent displacement on traces 1 and 2 occurred before the Lahontan highstand (15.5 ka).

Farther upslope on the same fan complex, trace 3 is defined by the truncation of a Qo fan surface and scarp of ~11.9 m (site 3; Figs. 6E, 6F; p2 in Fig. 6G). Our observations revealed no scarps within the intermediate-aged (Qi) fan surfaces at the ends of the mapped extent of trace 3. The most recent displacement here probably predates the Holocene (Figs. 6E, 6F).

At site 4 (Figs. 3, 6A, and 7) a small stream emanates from bedrock to cross the fault. Along the trace of this fault, a subdued ~1.5–2 m vertical scarp is preserved in an intermediate-aged fan surface (Figs. 7A, 7B). Based on the degradation of the scarp and its presence within a broad, deeply incised Qi fan surface, the last event on this particular trace was likely pre-Lahontan (before 15.5 ka). At this site, a fluvial terrace riser that marks the edge of the Qi surface appears to be left-laterally offset (Fig. 7). Using the upper and lower slope breaks of the southern terrace riser, we measure 1.6 ± 0.8 m of left-lateral offset in the SfM model (Fig. 7C). By dividing this offset measurement by the minimum age we determined for the fault trace (pre-Lahontan, 15.5 ka), a maximum bound of $<0.2 \pm 0.1$ mm/yr of left-lateral slip rate may be estimated for the fault, although the validity of the estimate should be questioned because the small displacement may be due to a single earthquake. There are multiple fault traces along this section of the fault (Fig. 3), which may also be accommodating left-lateral slip, thus while this is a maximum rate for this site, it is at best a minimum for the entirety of the zone.

Farther northeast of site 4 (Fig. 3), between Stagecoach and Silver Springs, a sequence of northeast-trending subparallel fault traces bend south-trending bedrock ridges, and cut through alluvium at elevations much higher than the pluvial highstand. The northernmost of these discontinuous faults is labeled site 5 in Figure 3 and images of it are shown in Figure 8. The three south-trending bedrock ridge crests, shown in Figure 8, are left-laterally offset 45 ± 10 m, 101 ± 20 m, and 53 ± 10 m, respectively, from west to east. A subdued scarp with ~0.5–1 m vertical separation (Figs. 8B, 8C) was observed in the field and is characterized by abundant burrows along the surface trace. Because the offset is limited to bedrock, the recency of these displacements is not clear, but further suggests a long-term left-lateral sense of strike-slip motion.

In sum, these discontinuous sets of faults along the Carson lineament show a long history of displacement, but a low rate of activity in the latest Quaternary. The vast majority of the scarps along the Carson lineament appear to be vertical with a down-to-the-southeast sense, do not show left-lateral displacement, and likely accommodate extension. However, the long-term

left-lateral displacement of bedrock ridges and the more recent displacement of two stream terraces at site 4 (Fig. 7) indicate that left-lateral motion is accommodated by the Carson lineament.

Wabuska Lineament

Observations

There are no known preexisting studies describing the fault geometry, nature, slip-rate, or rupture history of the Wabuska lineament from the past few decades.

The mapped traces of the discontinuous Quaternary faults are shown on a hillshade image and a simplified Quaternary map in Figure 9. Mapped fault traces are limited to the east of U.S. Route 95, are above the ca. 15.5 ka highstand of Lake Lahontan, and have a right-stepping en echelon pattern (Fig. 9). No Quaternary fault scarps are observed along the similar northeast-trending linear valley of Churchill Canyon on the west side of U.S. Route 95 (black arrows, Fig. 9), although we lack lidar data coverage for much of this lineation. The youngest alluvial units (Qy) are post-Lahontan fan and wash deposits; the mapped intermediate-aged (Qi) fans are >1 m above the active channels and have shoreline scarps and deposits on their surfaces (Figs. 10A, 10B). We subdivide the youngest alluvial unit into Qy1 and Qy2, as fault scarps are present within Qy2 and not within Qy1.

At site 6 (Figs. 9 and 10) we observe that the northeast-trending fault scarps cut predominantly through the intermediate-aged fan units and within Qy2 deposits (Figs. 10A, 10B). A larger scale lidar hillshade image (Fig. 10A) and photos Figures 10D and 10E provide a more detailed picture of the neotectonic and Quaternary characteristics of the fault morphology at site 6. At the western edge of site 6 (Fig. 10A), the Lahontan shorelines modify an intermediate-aged (Qi) fan deposit (Figs. 10A, 10B), allowing for a minimum age of the Lahontan highstand (ca. 15.5 ka) to be assigned to the intermediate (Qi) surface. Young fan units (Qy1 and Qy2) deposits cut or buried these intermediate (Qi) deposits and do not contain shoreline deposits. At site 6 (Fig. 10), a linear continuous fault scarp cuts across the front of an older fan (Qo) deposit and is expressed within the Qy2 alluvial deposits, which exhibit muted levee and channel topography and are younger than the Lahontan highstand (ca. 15.5 ka), based on the stratigraphic relations described here. Considering the intense damage from the reported 25 June 1933 Wabuska earthquake (~M6) (Reno Evening Gazette, 1933) and prior earthquakes recorded on other faults with similar magnitudes (M6 and M6.2) that have ruptured the ground surface (e.g., DeLong et al., 2015; Xu et al., 2015), one may speculate that the scarps were produced in 1933. Topographic profiles across the fault scarps show both uphill- and downhill-facing scarps with heights ranging from ~3 to 6 m (Fig. 10C). The linearity of the trace and reversal of scarp directions along strike indicate that the Wabuska lineament is a strike-slip fault.

A left-lateral sense of displacement is also observed at site 6 (Fig. 11) from displaced incised drainage channels and fan edges that are incised into an intermediate (Qi) fan, shown on the lidar image of Figure 11A.

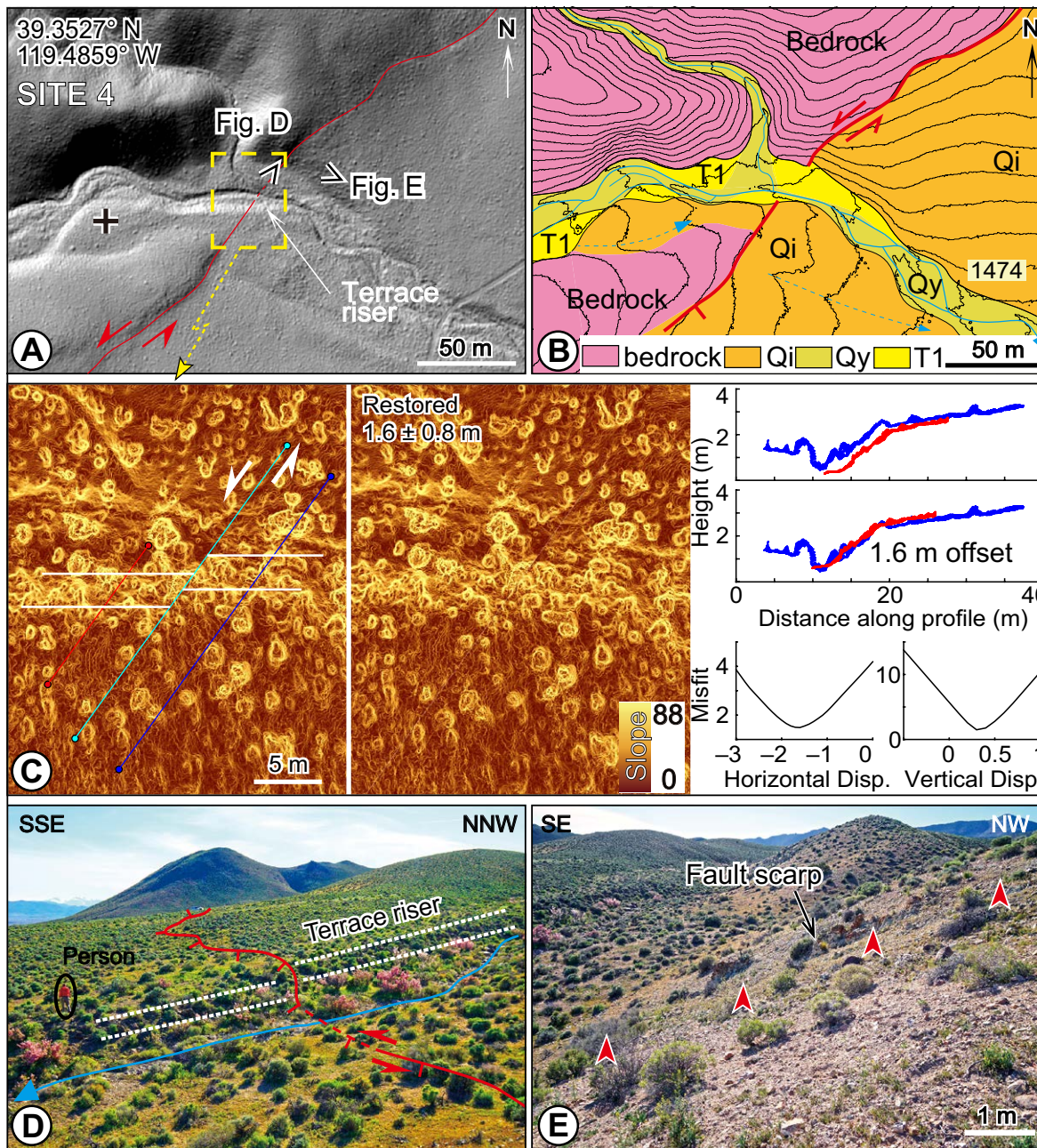


Figure 7. Displaced geomorphic features along the fault trace at site 4. (A) Lidar (light detection and ranging) hillshade image. (B) Quaternary map of area shown in A. See Figure 3 for unit descriptions and labels. (C) Structure-from-motion (SfM) derived slope map (left and middle) shows the left-lateral displaced terrace riser with 1.6 ± 0.8 m offset. Scale bar shows degree of slope angle. Topographic profiles (right) shows the left-lateral and vertical displacements (Disp.). The offsets were measured using LaDiCaoz_v2.1 (see text). (D and E) Field photos of the fault scarp. Perspectives of photos shown in A. Offset terrace riser is marked by dashed white lines in D and points of red arrowheads indicate the base of the fault scarp in E.

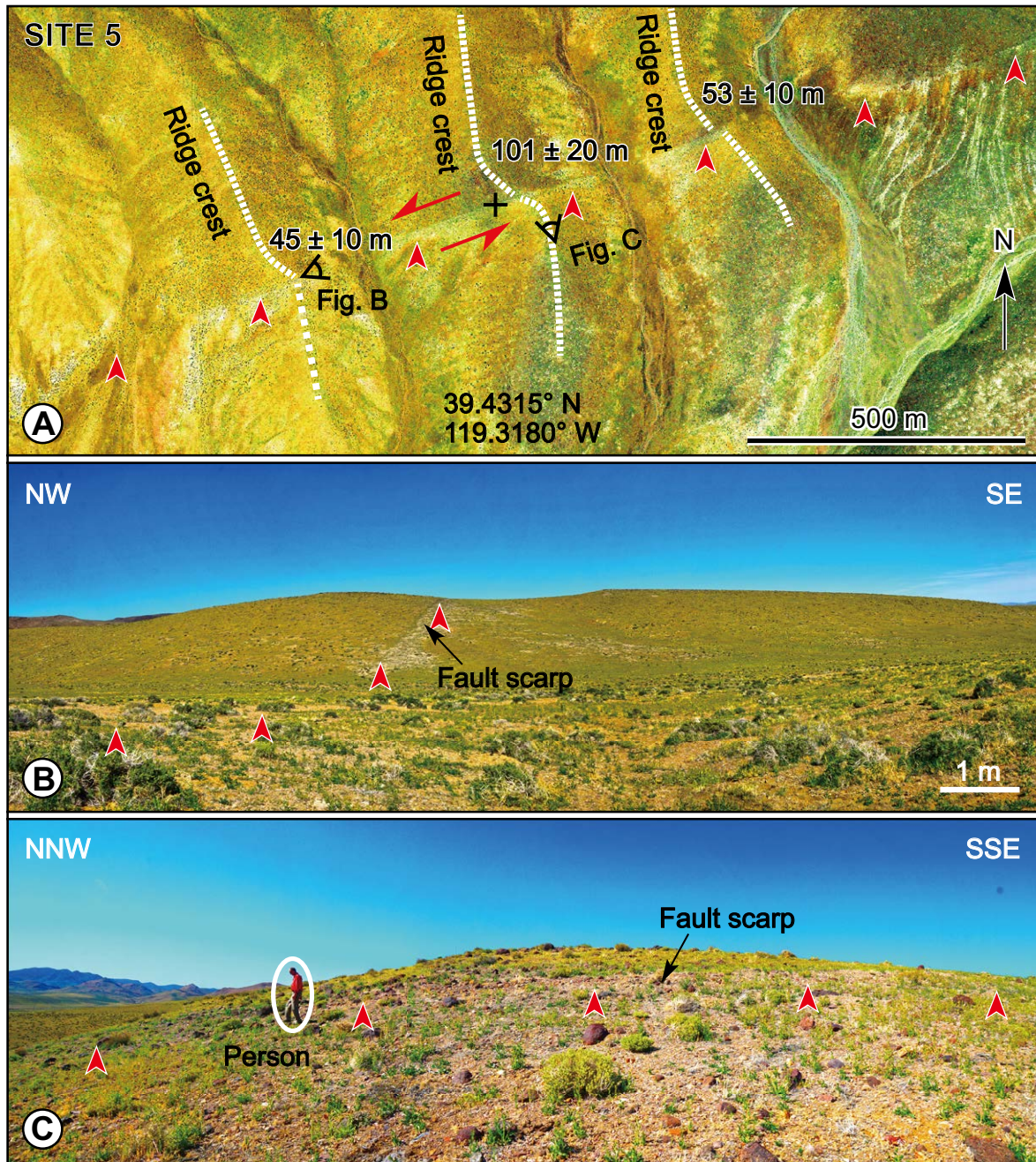
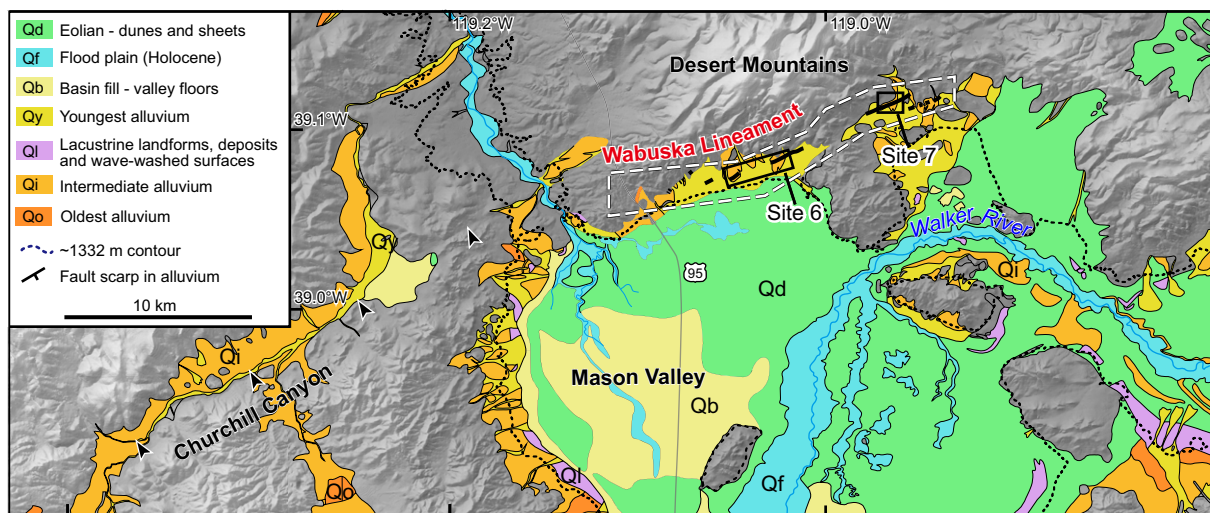


Figure 8. Displaced geomorphic features along the fault trace at site 5. Location outlined by box in Figure 3. (A) Google Earth imagery of the fault trace (red arrows) and displaced ridges (dashed white lines). Nearly linear ridge crests are consistent with left-lateral displacements of ~45–100 m. (B) Field photograph showing linearity fault trace. (C) Photo of youthful appearing fault scarp of ~0.5 m height. Points of red arrowheads are placed at base of the fault scarp.

Figure 9. Generalized map of Quaternary deposits along the Wabuska lineament shows locations of sites 6 and 7. The extent of lidar (light detection and ranging) coverage is indicated by the dashed white line. Thick black lines are active fault traces. Black arrows delineate the westward extent of the Wabuska lineament. Highstand of pluvial Lake Lahontan (~1332 m) is dashed black line. See Figure 3 for unit descriptions.



To better define the offset of some of these features, we produced SfM surface models and measured each using LaDiCaoz_v2.1 (Zielke et al., 2015; Haddon et al., 2016). Figures 11B and 11C display our offset measurement of a beheaded stream channel that we correlated to an active drainage across the fault showing 10.3 m of displacement. The drainage channel farther to the east, shown in Figures 11D and 11E, displays 10.7 ± 1 m of offset, however the channel is somewhat oblique to the northeast-trending fault trace, adding some uncertainty to the measurement. The measured displacements are likely the sum of multiple events, given that the expected amount of coseismic displacement for a fault of this length (~40 km) is $\ll 10$ m (Wells and Coppersmith, 1994; Wesnousky, 2008). Both of these offset measurements are derived from gullies cut into intermediate-aged (Qi) fan units, which are pre-Lahontan in age (before 15.5 ka), based on the presence of shoreline modification of the same surface farther to the west (Figs. 10A, 10B). A maximum slip rate for the fault may be approximated at $<0.7 \pm 0.1$ mm/yr if one assumes that displacement (10.3–10.7 m) of the gullies occurred after the ca. 15.5 ka Lahontan highstand.

Northeast of and along strike of the scarp at site 6, there is another northeast-trending fault scarp within a fan complex labeled site 7 in Figure 9. An enlarged lidar hillshade image of the scarp is shown in Figure 12A. The fault expression is quite clear, and appears in lidar imagery as a line of rounded hills along the southeast-facing scarps in the west, and as a thin white uphill-facing lineament cutting Qi alluvium to the east (Fig. 12A). The overall surface trace is slightly arcuate (Fig. 12B), trending approximately N64°E in the west and bending to N42°E at the eastern end. The Quaternary map in Figure 12B shows that alluvial deposits of old (Qo) and intermediate-aged (Qi) fans are cut by the fault, whereas the active washes (Qy) are not. Topographic profiles extracted from the lidar data across the oldest fan surface (Qo) show a scarp height of ~5–7 m,

whereas the height of upslope-facing scarps are ~1 m measured on the intermediate-aged fan surface (Fig. 12C). The alternate-facing fault scarps along strike further indicate a strike-slip origin. The muted levee and channel topography of the offset Qi surface suggests relative late Pleistocene or more recent displacement. We observed that the edge of a small stream channel was displaced ~2 m (Fig. 12E); this might be a result of the most recent earthquake along the fault.

In summary, the northeast-trending Wabuska lineament is characterized by discontinuous uphill- and downhill-facing fault scarps, implying strike-slip motion of faulting. Detailed analysis of the lidar imagery and our SfM models show that sinistral displacement has occurred on the Wabuska lineament and is preserved within the intermediate-aged fans. Fault scarps within the younger alluvium (Fig. 10) further show that this fault has likely produced earthquakes during the Holocene, and historical records of a 1933 earthquake may be able to be tied to this fault. Left-lateral offset measurements averaging ~10.5 m within an intermediate-aged fan surface correlated to a similar surface with the Lahontan shoreline (15.5 ka) modification provide a maximum left-lateral slip rate estimate of 0.7 ± 0.1 mm/yr.

DISCUSSION

Geomorphic Expression, Fault Motion, and Slip Rate during the Late Quaternary

Lidar has provided an opportunity to examine in detail the geomorphic expression of displacement along the east-trending Wabuska and Carson lineaments. Similar to previous observations along the Olinghouse lineament (Briggs and Wesnousky, 2005), the presence of scarps in late Pleistocene and

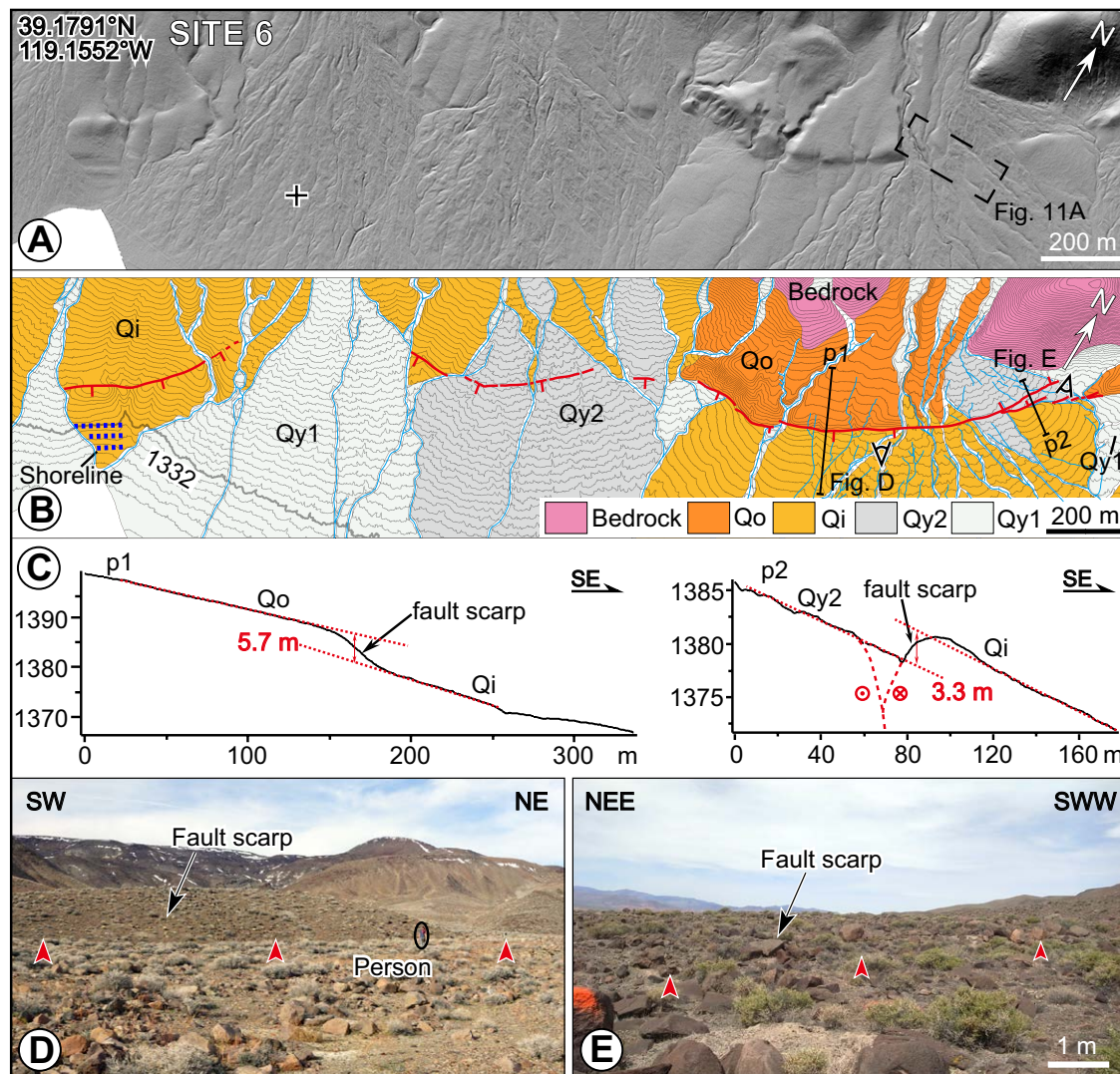


Figure 10. Displaced geomorphic features along the fault trace at site 6. (A) Lidar (light detection and ranging) hillshade image. (B) Quaternary map with active fault scarps shown as red lines (teeth on downthrown side) at the southeastern range front of the Desert Mountains (location outlined by box in Fig. 9). Contour interval is 2 m. See Figure 3 for unit descriptions. (C) Topographic profiles along lines p1 and p2 (shown in B) illustrate the height of scarps. The fault trace is characterized by both uphill- and downhill-facing fault scarps. (D) Field photograph showing southeast boundary of Qo surface. (E) Field photograph showing northwest-facing uphill fault scarp. Perspectives of photos in D and E are provided in B.

Holocene deposits shows elements of each to record active fault displacement. Likewise, the presence of relatively linear fault traces, bidirectional facing scarps, and left-lateral offsets of debris flow levees and channel thalwegs and margins further show each to exhibit left-lateral displacement. There are surprisingly few late Quaternary offset features observed along the faults; they are generally subdued in their preservation, and have afforded little opportunity to

assess the faults slip rates. To our knowledge, no slip rate along the Olinghouse fault based on the offset of a landform or rock of known age has been reported. Along the Carson lineament, the only measurable left-lateral offset is the <2 m channel margin displacement preserved in a pre-Holocene Qi (before 15.5 ka) fan surface preserved at site 4 (Fig. 7), but the validity of the $\sim 0.2 \pm 0.1$ mm/yr slip rate that arises from dividing the offset by the fan age is at best question-

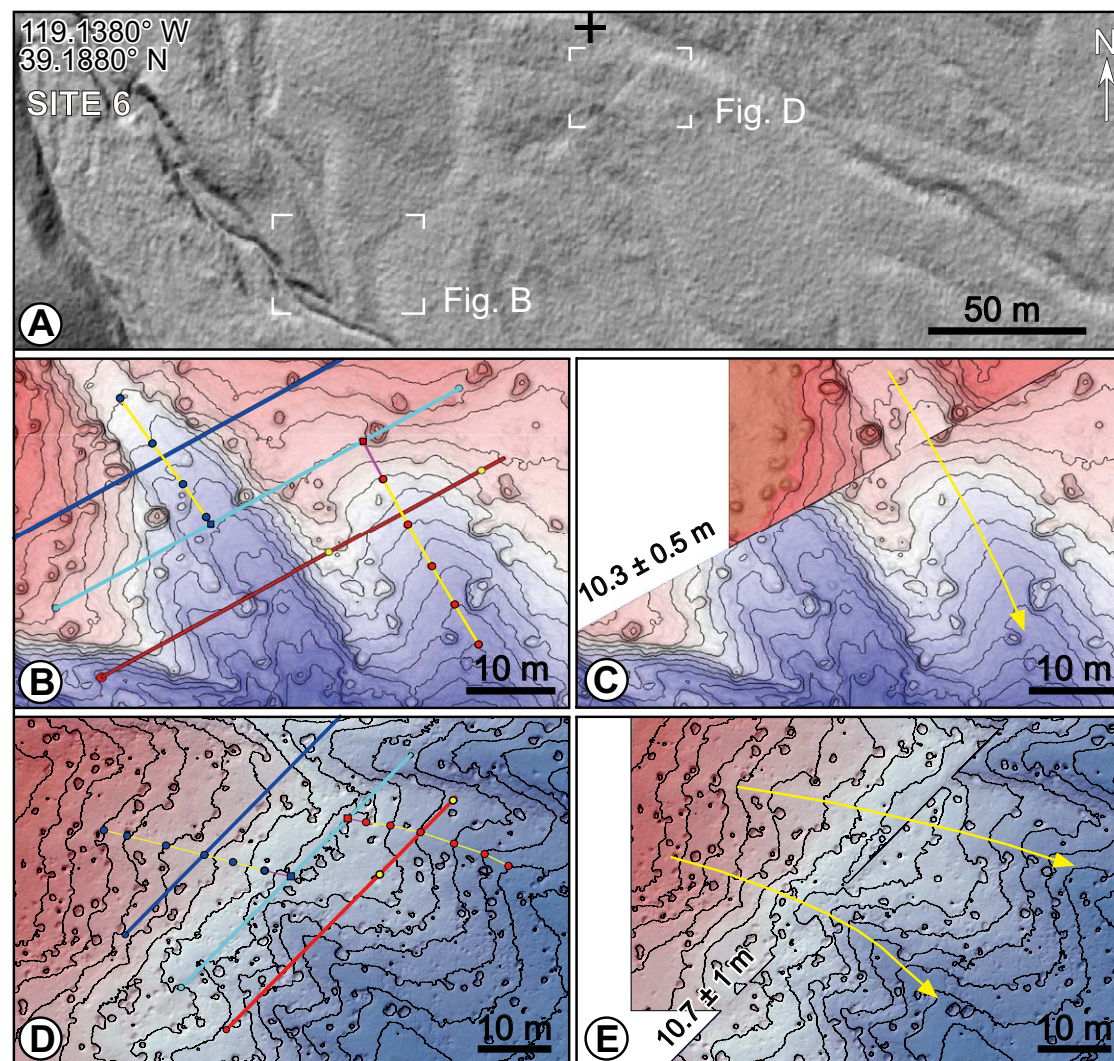


Figure 11. Left-lateral offset reconstruction at site 6. (A) Lidar (light detection and ranging) hillshade image (location outlined by dashed box in Fig. 10A). Pairs of images below show 0.5 m contour maps that illustrate the current and original (back slipped) location of stream channels crossing the Wabuska fault at sites outlined by white rectangles labeled B and D, respectively. Reconstructions of beheaded channels in B, C, D, and E are interpreted to indicate left-lateral offsets of ~10 m at each site. Elevation data are from the SfM (structure from motion) model. The offset measurements were conducted with LaDiCaoz_v2.1 (see text).

able because the small offset may be the result of only a single earthquake (e.g., Wells and Coppersmith, 1994; Wesnousky, 2008). There are multiple subparallel strands that are not accounted for in the estimated slip rate. Along the Wabuska lineament, the only opportunity to place a bound on the slip rate occurred with the ~10.5 m offset of the drainage channel incised into an intermediate-aged Qi fan surface (older than 15.5 ka) at site 6 (Fig 11), suggesting a low slip rate of <~0.7 mm/yr. This inability to place firm geologic limits on slip rates remains

for now a problem for both tectonic and seismic hazard analysis. Geodesy at this stage may give the most robust estimates of slip rates along these features. Predicted rates of lateral slip along the Carson and Wabuska faults are between 0.7 and 1.6 mm/yr (Hammond et al., 2011; Bormann et al., 2016), at the higher end and greater than the geologically estimated rates we report here.

While we are confident in our interpretations that the faults of each lineament are strike slip and left lateral, it should not be forgotten that scarps along the

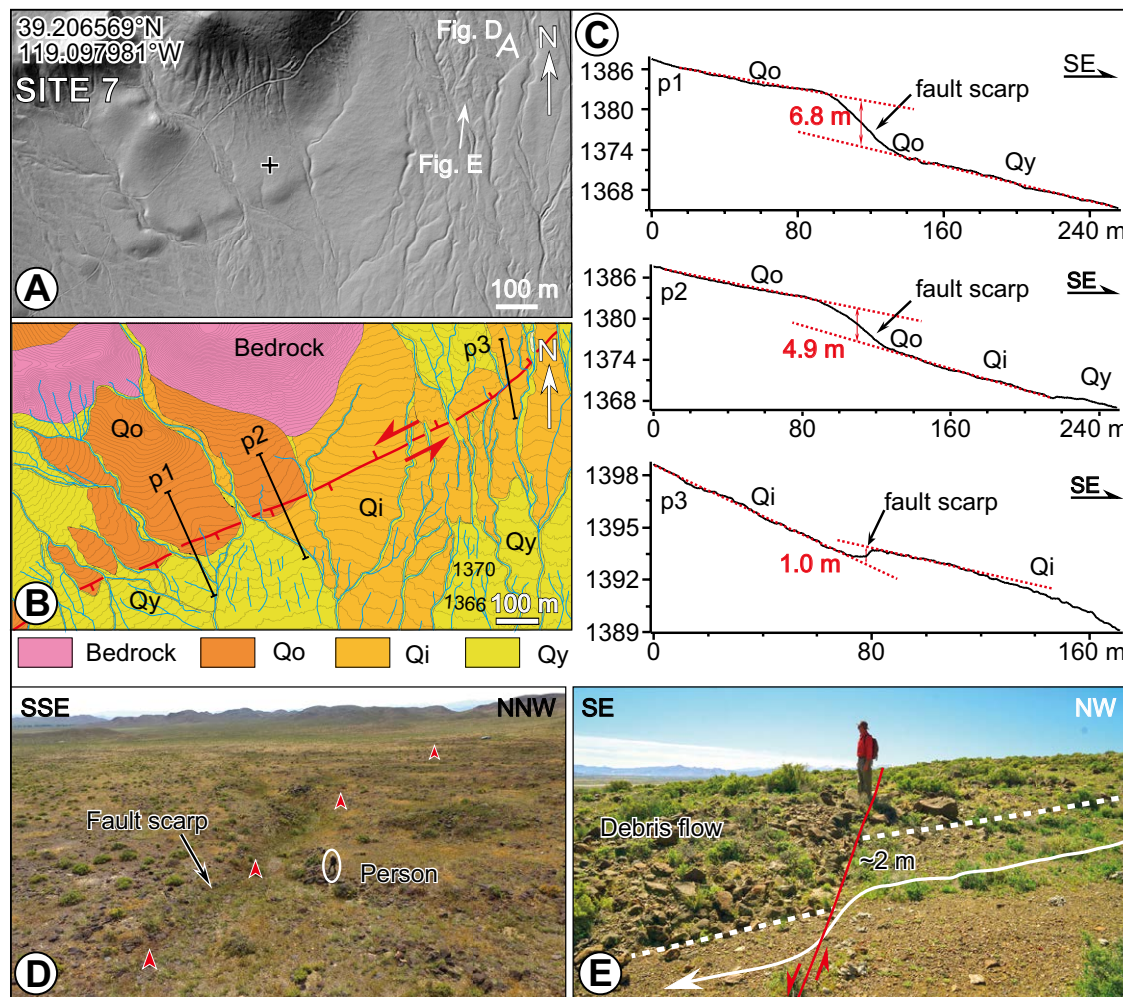


Figure 12. Displaced geomorphic features along the fault trace at site 7 (location outlined by box in Fig. 9). (A) Lidar (light detection and ranging) hillshade image. (B) Quaternary map showing active fault scarps (red lines, teeth on downthrown side). See Figure 3 for unit descriptions. The fault trace is characterized by alternate-facing scarp directions. (C) Topographic profiles along lines p1, p2, and p3 illustrating the scarp heights. (D) Field photograph shows character of southeast-facing fault scarp in field. Points of red arrowheads are placed on the downthrown side. (E) Field photograph showing a debris flow levy that is left-laterally displaced ~2 m by the fault trace. Perspectives of photos in D and E are indicated in A.

Carson lineament consistently face south, suggesting to us a consistent down-to-the-south normal component of motion. This should not be surprising in light of geodetic observations that show a northwest-directed component of extension along the length of the central and northern Walker Lane (Wesnousky, 2008).

Fault Geometry and Tectonic Implications

Within the Carson domain of the northern Walker Lane, transtensional dextral shear is accommodated in the absence of throughgoing right-lateral strike-slip faulting. The paleomagnetic measurements of Cashman and

Fontaine (2000) and Faulds et al. (2005), along with the GPS observations of Hammond et al. (2011) and Bormann et al. (2016), demonstrate that the crustal blocks between the Olinghouse fault and the Carson and Wabuska lineaments have undergone vertical axis clockwise rotations. The late Pleistocene–Holocene left-lateral faulting observed in this study suggests that these faults currently continue to accommodate the relative motion between these rotating blocks, and supports the predictions of left-lateral slip along the Carson and Wabuska lineaments (e.g., Wesnousky et al., 2012; Cashman and Fontaine, 2000). Recognition of faults and lineaments in this study combined with previous studies show that the western extent of the Carson and Wabuska

lineaments may intersect with the northernmost extent of the north-striking active range-bounding normal faults bounding the Carson and Smith Valleys (Stewart, 1999; Wesnousky et al., 2012; Fig. 1). A simplification of this geometric pattern is shown in Figures 13A and 13B and provides a conceptual idea of how these faults might work in concert to accommodate Walker Lane dextral shear by a linked system of block rotations and opening of adjacent asymmetric en echelon basins. The left-slip faults may also serve in part to passively accommodate a portion of the opening of the normal fault–bounded basins.

The Excelsior domain to the south is the one other area of the Walker Lane that exhibits left-lateral east-trending strike-slip faults (Figs. 1 and 13A). The left-lateral faults of the Excelsior domain transfer slip to the east in the form of a right step (Wesnousky, 2005a, 2005b; Fig. 13C). Specifically, the Excelsior domain transfers slip from the northwest-trending strike-slip faults of the southern Walker Lane to the northwest-trending strike-slip faults of the central Walker Lane (Fig. 13C). The accommodation of Walker Lane shear in the Carson domain is considerably different. In the Carson domain, Walker Lane slip does not step right or left, instead dextral shear is transferred in the absence of

a stepover from the northwest-striking right-lateral faults of the central Walker Lane to the northwest-striking right-lateral faults of the northern Walker Lane (Fig. 13A).

In sum, while it appears that east-striking left-slip faults are accommodating active vertical axis crustal rotations in both the Excelsior and Carson domains (e.g., Cashman and Fontaine, 2000; Wesnousky, 2005a), it seems that the geometry and thus mechanical genesis of the left-slip faults and development of basins in each region that reflect the accommodation of the crustal rotations have evolved quite differently.

The Walker Lane is an element of the Pacific–North American plate margin and in this sense a part of the San Andreas fault system. It has been interpreted that the Walker Lane shear zone represents an incipient plate boundary, whereby relative motion currently focused along the San Andreas fault proper is commencing and will ultimately migrate continentward to the Walker Lane (Faulds et al., 2005). In Wesnousky (2005a, 2005b) it was further noted that the displacement along the Walker Lane is currently transtensional, whereas it is transpressional along all but the southernmost San Andreas fault. The occurrence of vertical axis rotations and development of extensional basins along a strike-slip system require that it be transtensional and not transpressional. A large amount of block rotation and basin development occurred along the southern San Andreas in the Miocene, when ongoing shear deformation was transtensional rather than transpressional (Luyendyk, 1991). It is a testable hypothesis, although well beyond the scope of this effort, to suggest that older basins preserved astride or adjacent to the San Andreas formed in the same manner as those in the Excelsior or Carson domains. Examination of other major continental strike-slip zones such as the great Anatolian fault of Turkey, the Altyn Tagh of Tibet, the Denali fault system of Alaska, and the Alpine fault system of New Zealand may provide observations to test the hypothesis.

CONCLUSIONS

It has generally been assumed that the northeast-trending Carson and Wabuska lineaments within the Carson domain have accommodated left-lateral motion (e.g., Shawe, 1965; Rogers, 1975; Slemmons et al., 1979; Cashman and Fontaine, 2000). The observations presented in this paper illustrate that faults within each of the lineaments, along with the Olinghouse fault, are active, cut late Pleistocene deposits, and exhibit apparently low (probably <1 mm/yr) left-lateral slip rates. The northeast-striking active left-lateral faults of the Carson domain are similar to those of the Excelsior domain in that they interrupt the northwestern structural grain of the Walker Lane. The two fault systems differ in the sense that the faults of the Excelsior trend can be attributed to a distinct right step in the northwestern right-lateral faulting of the Walker Lane, whereas the left-lateral faults of the Carson domain appear to be accommodating motion arising from or in concert with block rotations and the opening of large normal fault–bounded basins that are west of the northwest-trending zone of right-lateral faults composing the central Walker Lane at that latitude.

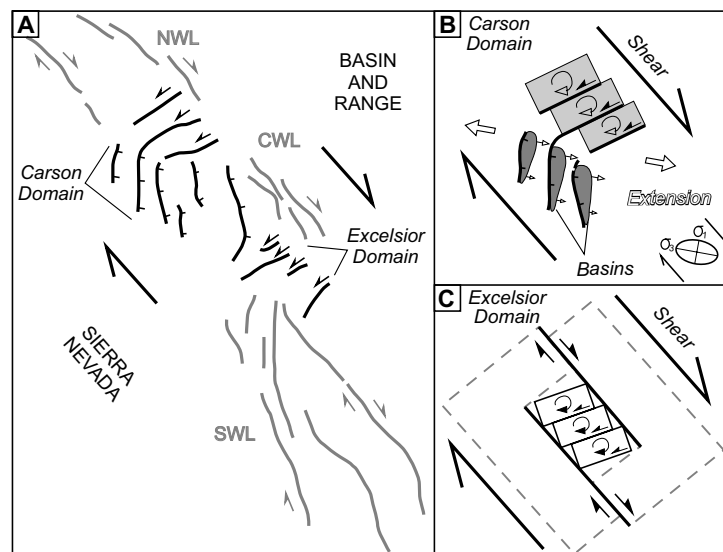


Figure 13. Fault geometry of Walker Lane and simplified models showing the accommodation of Walker Lane shear in the Carson and Excelsior domains. (A) Simplified line map of Walker Lane faults. The northwest-striking right-lateral faults of the southern Walker Lane (SWL), central Walker Lane (CWL), and northern Walker Lane (NWL) are shown as gray lines. The northeast-striking left-lateral faults and north-striking normal faults within the Carson and Excelsior domains are shown as black lines. (B, C) Conceptual sketches illustrating how accommodation of northwest-directed right shear in the Carson and Excelsior domains differ in the sense that left-lateral faults of the Excelsior trend can be attributed to block rotations within a distinct right step in the northwestern right-lateral faulting of the Walker Lane, whereas the left-lateral faults of the Carson domain appear to be accommodating motion arising from or in concert with block rotations and the opening of large normal fault–bounded basins.

ACKNOWLEDGMENTS

This research was supported in part by National Science Foundation (NSF) grant EAR-1419724. The lidar data for this study were funded by the NSF and collected and processed by the National Center for Airborne Laser Mapping (NCALM). The efforts and reviews of Nicolas Barth, and editors Jeff Lee, Raymond Russo, and an anonymous reviewer are most appreciated and helped improve the paper immensely. I thank the University of Nevada, Reno, for hosting me during this study. I also thank all the faculty, staff, and graduate students at the Department of Geology and those at the Nevada Seismological Laboratory who have helped my understanding of this region. This is Center for Neotectonic Studies Contribution 72.

REFERENCES CITED

- Adams, K.D., and Wesnousky, S.G., 1999, The Lake Lahontan highstand: Age, surficial characteristics, soil development, and regional shoreline correlation: *Geomorphology*, v. 30, p. 357–392, doi:10.1016/S0169-555X(99)00031-8.
- Angster, S., Wesnousky, S.G., Huang, W.L., Kent, G., Nakata, T., and Goto, H., 2016, Application of UAV photography to refining the slip rate on the Pyramid lake fault zone, Nevada: *Bulletin of the Seismological Society of America*, v. 106, p. 785–798, doi:10.1785/0120150144.
- Bell, J.W., 1981, Quaternary Fault Map of the Reno 1 × 2 Quadrangle, Nevada-California: U.S. Geological Survey Open-File Report 81-892, 63 p.
- Bell, J.W., 1984, Quaternary Fault Map of Nevada, Reno Sheet: Nevada Bureau of Mines and Geology Map 79, scale 1:250,000.
- Bell, J.W., Caskey, S.J., Ramelli, A.R., and Guerrieri, L., 2004, Pattern and rates of faulting in the central Nevada seismic belt, and paleoseismic evidence for prior beltlike behavior: *Bulletin of the Seismological Society of America*, v. 94, p. 1229–1254, doi:10.1785/0120032226.
- Bennett, R.A., Wernicke, B.P., Niemi, N.A., Friedrich, A.M., and Davis, J.L., 2003, Contemporary strain rates in the northern Basin and Range province from GPS data: *Tectonics*, v. 22, 1008, doi:10.1029/2001TC001355.
- Bonham, H.F., 1969, *Geology and Mineral Deposits of Washoe and Storey Counties, Nevada*: Nevada Bureau of Mines and Geology Bulletin 70, 140 p.
- Bormann, J.M., Hammond, W.C., Kreemer, C., and Blewitt, G., 2016, Accommodation of missing shear strain in the Central Walker Lane, western North America: Constraints from dense GPS measurements: *Earth and Planetary Science Letters*, v. 440, p. 169–177, doi:10.1016/j.epsl.2016.01.015.
- Briggs, R.W., and Wesnousky, S.G., 2001, Paleoseismic evidence for repeated Holocene earthquakes on the Olinghouse fault zone, western Nevada: *American Geophysical Union 2001 Fall Meeting*, abs. S52D–0678.
- Briggs, R.W., and Wesnousky, S.G., 2004, Late Pleistocene fault slip rate, earthquake recurrence, and recency of slip along the Pyramid Lake fault zone, northern Walker Lane, United States: *Journal of Geophysical Research*, v. 109, B08402, doi:10.1029/2003JB002717.
- Briggs, R.W., and Wesnousky, S.G., 2005, Late Pleistocene and Holocene paleoearthquake activity of the Olinghouse fault zone, Nevada: *Bulletin of the Seismological Society of America*, v. 95, p. 1301–1313, doi:10.1785/0120040129.
- Bull, W.B., 1991, *Geomorphic Responses to Climatic Change*: New York, Oxford University Press, 326 p.
- Callaghan, E., and Gianella, V.P., 1935, The earthquake of January 30, 1934, at Excelsior Mountains, Nevada: *Bulletin of the Seismological Society of America*, v. 25, p. 161–168.
- Carlson, C.W., and Faulds, J.E., 2016, Translation vs. rotation: The battle for enigmatic dextral-shear accommodation in the Walker Lane, western Nevada, USA: *Geological Society of America Abstracts with Programs*, v. 48, no. 7, no. 117–10, doi:10.1130/abs/2016AM-287867.
- Carlson, C.W., Pluhar, C.J., Glen, J.M.G., and Farnier, M.J., 2013, Kinematics of the west-central Walker Lane: Spatially and temporally variable rotations evident in the late Miocene Stanislaus Group: *Geosphere*, v. 9, p. 1530–1551, doi:10.1130/GES00955.1.
- Cashman, P.H., and Fontaine, S.A., 2000, Strain partitioning in the northern Walker Lane, western Nevada and northeastern California: *Tectonophysics*, v. 326, p. 111–130, doi:10.1016/S0040-1951(00)00149-9.
- DeLong, S.B., Lienkaemper, J.J., Pickering, A.J., and Avdievitch, N.N., 2015, Rates and patterns of surface deformation from laser scanning following the South Napa earthquake, California: *Geosphere*, v. 11, p. 2015–2030, doi:10.1130/GES01189.1.
- DePolo, C.M., 2014, Collaborative Research Between the Nevada Bureau of Mines and Geology and the USGS on the Paleoseismic History of the Kings Canyon Fault Zone, Nevada: Earthquake Hazards Program Final Technical Report, 72 p., U.S. Geological Survey EHP Award No. G12AP20047.
- Dixon, T.H., Robaudo, S., Lee, J., and Reheis, M.C., 1995, Constraints on present-day Basin and Range deformation from space geodesy: *Tectonics*, v. 14, p. 755–772, doi:10.1029/95TC00931.
- Dokka, R.K., and Travis, C.J., 1990, Role of the eastern California shear zone in accommodating Pacific–North American plate motion: *Geophysical Research Letters*, v. 17, p. 1323–1326, doi:10.1029/GL017i009p01323.
- Faulds, J.E., and Henry, C.D., 2008, Tectonic influences on the spatial and temporal evolution of the Walker Lane: An incipient transform fault along the evolving Pacific–North American plate boundary, *in* Spencer, J.E., and Titley, S.R., eds., *Ores and Orogenesis: Circum-Pacific Tectonics, Geologic Evolution, and Ore Deposits*: Arizona Geological Society Digest 22, p. 437–470.
- Faulds, J.E., Henry, C.D., and Hinz, N.H., 2003, Kinematics and cumulative displacement across the northern Walker Lane, an incipient transform fault, northwest Nevada and northeast California: *Geological Society of America Abstracts with Programs*, v. 35, no. 6, p. 305.
- Faulds, J.E., Henry, C.D., and Hinz, N.H., 2005, Kinematics of the northern Walker Lane: An incipient transform fault along the Pacific–North American plate boundary: *Geology*, v. 33, p. 505–508, doi:10.1130/G21274.1.
- Ferguson, H.G., and Muller, S.W., 1949, *Structural Geology of the Hawthorne and Tonopah quadrangles, Nevada*: U.S. Geological Survey Professional Paper 216, 55 p.
- Frankel, K.L., et al., 2007a, Cosmogenic ¹⁰Be and ³⁶Cl geochronology of offset alluvial fans along the northern Death Valley fault zone: Implications for transient strain in the eastern California shear zone: *Journal of Geophysical Research*, v. 112, B06407, doi:10.1029/2006JB004350.
- Frankel, K.L., Dolan, J.F., Finkel, R.C., Owen, L.A., and Hoefft, J.S., 2007b, Spatial variations in slip rate along the Death Valley–Fish Lake Valley fault system determined from LiDAR topographic data and cosmogenic ¹⁰Be geochronology: *Geophysical Research Letters*, v. 34, L18303, doi:10.1029/2007GL030549.
- Haddon, E.K., Amos, C.B., Zielke, O., Jayko, A.S., and Bürgmann, R., 2016, Surface slip during the large Owens Valley earthquake: *Geochemistry, Geophysics, Geosystems*, v. 17, p. 2239–2269, doi:10.1002/2015GC006033.
- Hammond, W.C., and Thatcher, W., 2007, Crustal deformation across the Sierra Nevada, northern Walker Lane, Basin and Range transition, western United States measured with GPS, 2000–2004: *Journal of Geophysical Research*, v. 112, B05411, doi:10.1029/2006JB004625.
- Hammond, W.C., Blewitt, G., and Kreemer, C., 2011, Block modeling of crustal deformation of the northern Walker Lane and Basin and Range from GPS velocities: *Journal of Geophysical Research*, v. 116, B04440, doi:10.1029/2010JB007817.
- Hanks, T.C., Bucknam, R.C., Lajoie, K.R., and Wallace, R.E., 1984, Modification of wave-cut and faulting-controlled landforms: *Journal of Geophysical Research*, v. 89, p. 5771–5790, doi:10.1029/JB089iB07p05771.
- Henry, C.D., Faulds, J.E., and dePolo, C.M., 2007, Geometry and timing of strike-slip and normal faults in the northern Walker Lane, northwestern Nevada and northeastern California: Strain partitioning or sequential extensional and strike-slip deformation?, *in* Roeske, S.M., et al., eds., *Exhumation Associated with Continental Strike-Slip Fault Systems*: Geological Society of America Special Paper 434, p. 59–79, doi:10.1130/2007.2434(04).
- Hickman, R.G., Craddock, C., and Sherwood, K.W., 1978, The Denali fault system and the tectonic development of southern Alaska: *Tectonophysics*, v. 47, p. 247–257, 253–273, doi:10.1016/0040-1951(78)90033-1.
- Hoefft, J.S., and Frankel, K.L., 2010, Temporal variations in extension rate on the Lone Mountain fault and strain distribution in the eastern California shear zone–Walker Lane: *Geosphere*, v. 6, p. 917–936, doi:10.1130/GES00603.1.
- Koehler, R.D., and Wesnousky, S.G., 2011, Late Pleistocene regional extension rate derived from earthquake geology of late Quaternary faults across the Great Basin, Nevada, between 38.5°N and 40°N latitude: *Geological Society of America Bulletin*, v. 123, p. 631–650, doi:10.1130/B30111.1.
- Locke, A., Billingsley, P., and Mayo, E.B., 1940, Sierra Nevada tectonic patterns: *Geological Society of America Bulletin*, v. 51, p. 513–539, doi:10.1130/GSAB-51-513.
- Luyendyk, B.P., 1991, A model for Neogene crustal rotations, transtension, and transpression in southern California: *Geological Society of America Bulletin*, v. 103, p. 1528–1536, doi:10.1130/0016-7606(1991)103<1528:AMFNCR>2.3.CO;2.
- Mortimer, N., et al., 2017, Zealandia: Earth's hidden continent: *GSA Today*, v. 27, no. 3, p. 27–35, doi:10.1130/GSATG321A.1.

- Nagorsen-Rinke, S., Lee, J., and Calvert, A., 2013, Pliocene sinistral slip across the Adobe Hills, eastern California-western Nevada: Kinematics of fault slip transfer across the Mina deflection: *Geosphere*, v. 9, p. 37–53, doi:10.1130/GES00825.1.
- Norris, R.J., and Toy, V.G., 2014, Continental transforms: A view from the Alpine Fault: *Journal of Structural Geology*, v. 64, p. 3–31, doi:10.1016/j.jsg.2014.03.003.
- Oldow, J.S., Aiken, C.L.V., Hare, J.L., Ferguson, J.F., and Hardyman, R.F., 2001, Active displacement transfer and differential block motion within the Central Walker Lane, western Great Basin: *Geology*, v. 29, p. 19–22, doi:10.1130/0091-7613(2001)029<0019:ADTADB>2.0.CO;2.
- Ramelli, A.R., Bell, J.W., dePolo, C.M., and Yount, J.C., 1999, Large-magnitude, late Holocene earthquakes on the Genoa fault, west-central Nevada and eastern California: *Bulletin of the Seismological Society of America*, v. 89, p. 1458–1472.
- Reheis, M.C., and Dixon, T.H., 1996, Kinematics of the Eastern California shear zone: Evidence for slip transfer from Owens and Saline Valley fault zones to Fish Lake Valley fault zone: *Geology*, v. 24, p. 339–342, doi:10.1130/0091-7613(1996)024<0339:KOTECES>2.3.CO;2.
- Reno Evening Gazette, 1933, Quake relieves quiet Sunday: *Reno Evening Gazette Newspaper Archives*, 26 June 1933, v. 23, no. 4, p. 3.
- Rogers, D.K., 1975, The Carson Lineament: Its influence on recent left-lateral faulting near Carson City, Nevada: *Geological Society of America Abstracts with Programs*, v. 7, no. 7, p. 1250.
- Sanders, C.O., and Slemmons, D.B., 1979, Recent crustal movements in the central Sierra Nevada–Walker Lane region of California–Nevada: Part iii, the Olinghouse fault zone: *Tectonophysics*, v. 52, p. 585–597, doi:10.1016/0040-1951(79)90273-7.
- Sarmiento, A.C., Wesnousky, S.G., and Bormann, J.M., 2011, Paleoseismic trenches across the Sierra Nevada and Carson range fronts in Antelope Valley, California, and Reno, Nevada: *Bulletin of the Seismological Society of America*, v. 101, p. 2542–2549, doi:10.1785/0120100176.
- Şengör, A.M.C., Tüysüz, O., Imren, C., Sakiç, M., Eyidoğan, H., Görür, N., Pichon, X.L., and Rangin, C., 2005, The North Anatolian fault: A new look: *Annual Review of Earth and Planetary Sciences*, v. 33, p. 37–112, doi:10.1146/annurev.earth.32.101802.120415.
- Shawe, D.R., 1965, Strike-slip control of Basin-Range structure indicated by historical faults in western Nevada: *Geological Society of America Bulletin*, v. 76, p. 1361–1378, doi:10.1130/0016-7606(1965)76[1361:SCOBIS]2.0.CO;2.
- Slemmons, D.B., Van Wormer, D., Bell, E.J., and Silberman, M.L., 1979, Recent crustal movements in the Sierra Nevada–Walker Lane region of California–Nevada: Part i, rate and style of deformation: *Tectonophysics*, v. 52, p. 561–570, doi:10.1016/0040-1951(79)90271-3.
- Stewart, J.H., 1980, *Geology of Nevada*: Nevada Bureau of Mines and Geology Special Publication 4, 136 p.
- Stewart, J.H., 1985, East-trending dextral faults in the western Great Basin: An explanation for anomalous trends of pre-Cenozoic strata and Cenozoic faults: *Tectonics*, v. 4, p. 547–564, doi:10.1029/TC004i006p00547.
- Stewart, J.H., 1988, Tectonics of the Walker Lane belt, western Great Basin: Mesozoic and Cenozoic deformation in a zone of shear, *in* Ernst, W.G., *Metamorphism and Crustal Evolution of the Western United States: Ruby Volume VII*: Englewood Cliffs, New Jersey, Prentice Hall, p. 685–713.
- Stewart, J.H., 1999, *Geologic Map of the Carson City 30 × 60 Minute Quadrangle, Nevada*: Nevada Bureau of Mines and Geology University Map 118, scale 1:100,000.
- Stockli, D.F., Surpless, B.E., Dumitru, T.A., and Farley, K.A., 2002, Thermochronological constraints on the timing and magnitude of Miocene and Pliocene extension in the central Wassuk Range, western Nevada: *Tectonics*, v. 21, p. 10–11–10–19, doi:10.1029/2001TC001295.
- Surpless, B.E., Stockli, D.F., Dumitru, T.A., and Miller, E.L., 2002, Two-phase westward encroachment of Basin and Range extension into the northern Sierra Nevada: *Tectonics*, v. 21, p. 2–1–2–10, doi:10.1029/2000TC001257.
- Trexler, D.T., and Bell, J.W., 1979, *Carson City Quadrangle Earthquake Hazards Map*: Nevada Bureau of Mines and Geology Map 1A1, scale 1:24,000.
- Unruh, J., Humphrey, J., and Barron, A., 2003, Transtensional model for the Sierra Nevada frontal fault system, eastern California: *Geology*, v. 31, p. 327–330, doi:10.1130/0091-7613(2003)031<0327:TMFTSN>2.0.CO;2.
- Wells, D.L., and Coppersmith, K.J., 1994, New empirical relationships among magnitude, rupture length, rupture width, rupture area, and surface displacement: *Bulletin of the Seismological Society of America*, v. 84, p. 974–1002.
- Wesnousky, S.G., 2005a, Active faulting in the Walker Lane: *Tectonics*, v. 24, TC3009, doi:10.1029/2004TC001645.
- Wesnousky, S.G., 2005b, The San Andreas and Walker Lane fault systems, western North America: Transpression, transtension, cumulative slip and the structural evolution of a major transform plate boundary: *Journal of Structural Geology*, v. 27, p. 1505–1512, doi:10.1016/j.jsg.2005.01.015.
- Wesnousky, S.G., 2008, Displacement and geometrical characteristics of earthquake surface ruptures: Issues and implications for seismic-hazard analysis and the process of earthquake rupture: *Bulletin of the Seismological Society of America*, v. 98, p. 1609–1632, doi:10.1785/0120070111.
- Wesnousky, S.G., and Caffee, M., 2011, Range-bounding normal fault of Smith Valley, Nevada: Limits on age of last surface-rupture earthquake and late Pleistocene rate of displacement: *Bulletin of the Seismological Society of America*, v. 101, p. 1431–1437, doi:10.1785/0120100238.
- Wesnousky, S.G., and Jones, C.H., 1994, Oblique slip, slip partitioning, spatial and temporal changes in the regional stress field, and the relative strength of active faults in the Basin and Range, western United States: *Geology*, v. 22, p. 1031–1034, doi:10.1130/0091-7613(1994)022<1031:OSSPSA>2.3.CO;2.
- Wesnousky, S.G., Bormann, J.M., Kreemer, C., Hammond, W.C., and Brune, J.N., 2012, Neotectonics, geodesy, and seismic hazard in the Northern Walker Lane of western North America: Thirty kilometers of crustal shear and no strike-slip?: *Earth and Planetary Science Letters*, v. 329–330, p. 133–140, doi:10.1016/j.epsl.2012.02.018.
- Xu, X.W., Xu, C., Yu, G.H., Wu, X.Y., Li, X., and Zhang, J.G., 2015, Primary surface ruptures of the Ludian Mw 6.2 earthquake, southeastern Tibetan plateau, China: *Seismological Research Letters*, v. 86, p. 1622–1635, doi:10.1785/0220150038.
- Yin, A., et al., 2002, Tectonic history of the Altyn Tagh fault system in northern Tibet inferred from Cenozoic sedimentation: *Geological Society of America Bulletin*, v. 114, p. 1257–1295, doi:10.1130/0016-7606(2002)114<1257:THOTAT>2.0.CO;2.
- Zielke, O., Klinger, Y., and Arrowsmith, J.R., 2015, Fault slip and earthquake recurrence along strike-slip faults—Contributions of high-resolution geomorphic data: *Tectonophysics*, v. 638, p. 43–62, doi:10.1016/j.tecto.2014.11.004.